Design and Analysis of a MEMS Comb Vibratory Gyroscope

Haifeng Dong, Xingguo Xiong
Department of Electrical and Computer Engineering,
University of Bridgeport, Bridgeport, CT 06604

Abstract

MEMS (Micro-electro-mechanical Systems) refer to devices or systems integrated with electrical and mechanical components in the scale of microns. Due to its small size, low cost, low power consumption and high efficiency, MEMS technology has been widely used in many fields. In this paper, a novel comb-driven, differential capacitance sensing MEMS vibratory gyroscope based on glass-silicon-glass structure is proposed. The gyroscope is activated to vibrate along X axis by electrostatic comb driving. If an angular velocity along Y axis is experienced, the Coriolis force along Z axis activates the sensing vibration of the central mass along Y axis. The size of the driving beams and sensing beams are carefully chosen to reduce the frequency mismatch in two directions, thus increasing the gyroscope sensitivity. The working principle and dynamic analysis of this gyroscope are given and a set of optimized design parameters are derived based on the analysis. ANSYS FEM simulation is used to find out the device frequency and verify the theoretical prediction. The fabrication process flow of the MEMS gyroscope is also proposed. The microgyroscope can be used for inertial navigation in many applications, such as automobile, aerospaceship, microsatellite, consumer products, etc.

I. Introduction

MEMS gyroscopes are used to sense the angular velocity experienced by a system. They have been good examples for MEMS commercial products and have made their way into various applications [1]-[3]. One of the most common uses for MEMS gyroscopes is spacecraft orientation. In this case gyroscopes are used to sense angular velocity of the spacecrafts. A processor will analyze the magnitude and direction of the angular rate and decide on how to adjust the traveling direction to pull the spaceship back to its original course. MEMS gyroscopes are quickly replacing conventional gyroscopes in inertial navigation. The reason behind this increasing popularity is, the MEMS gyroscopes are much smaller, lighter, more reliable and are produced for a fraction of the cost of the conventional gyroscopes.

Among different kinds of MEMS gyroscopes, electrostatic driving, capacitance sensing microgyroscope is a very attractive category [4]-[5]. These gyroscopes use electrostatic comb drive to activate the device in X direction. If there is an angular velocity along Y direction, the mass will vibrate along Z direction due to Coriolis force. By measuring the capacitance change between the moving mass and fixed electrode plate, the value of angular velocity can be known. In vibrating gyroscopes, reducing the mismatch between the resonant frequencies of the driving and detection modes is important to attain high detection sensitivity. However, as the mismatch decreases, the mechanical coupling between the two modes makes operation more and more unstable. In [6]-[11], vibratory microgyroscopes with independent beams for driving and sensing are reported. With driving and sensing beams sensitive to vibrations along different directions, these microgyroscopes can significantly reduce mechanical coupling effect. Due to the small sensing mass and small size of the MEMS gyroscopes, the signal detection is always a very challenging issue. Z-axis vibratory gyroscopes [6]-[8] usually use comb fingers to sense the capacitance change, typically having device capacitance in the range of pF (10^{-12} F) and capacitance change in the range of fF (10^{-15} F). X/Y-axis vibratory gyroscopes [9]-[11] vibrate laterally through push-pull comb drive and detect the displacement of the mass vertically. These microgyroscopes have a lager capacitive overlap area than

Z-axis vibratory gyroscopes, however, suffered from squeeze film air damping.

The design in this paper is an X/Y-axis microgyroscope with some methods to increase the device sensitivity. First, the sensing mass is connected to folded sensing beams, which can increase the effective beam length and increase the displacement of the sensing mass. Second, by using a maskless etching technique, the beam thickness of the sensing beam can be reduced to be much thinner than the device thickness. In this way, the sensing vibration amplitude and sensing capacitance can be greatly increased. Furthermore, the device is released by DRIE etching, thus the device thickness can be as thick as a silicon wafer. Finally, the device uses differential capacitance sensing instead of sensing a single capacitance change, which can further improve the accuracy of signal detection.

II. Working principle

A vibratory gyroscope generally has two perpendicular vibration modes: driving mode and sensing mode, which can be simplified as a mass suspended by springs along two orthogonal directions, as shown in Figure 1.

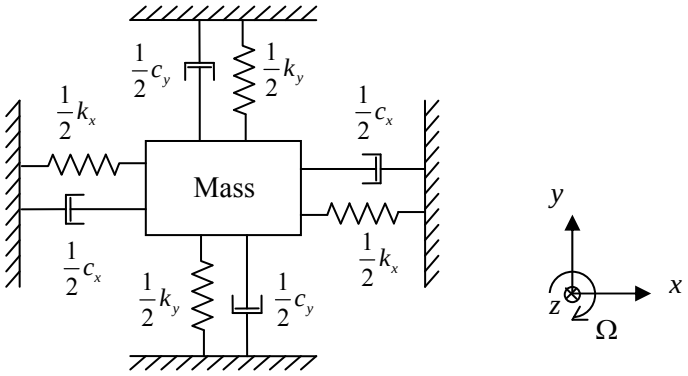

Figure 1. Simple model of a vibratory microgyroscope

When the mass is driven along the x-direction by an external force ($F(t) = F_0 \cos \omega_d t$), and it is subjected to a constant angular velocity (Ω), a Coriolis force ($F_c(t) = 2m\Omega \frac{dx(t)}{dt}$) is induced in y-direction. In this case, the equation of movement is

$$m\frac{d^2x(t)}{dt^2} + c_x\frac{dx(t)}{dt} + k_x x(t) = F_0 \cos \omega_d t \tag{1}$$

$$m\frac{d^2y(t)}{dt^2} + c_y\frac{dy(t)}{dt} + k_y y(t) = 2m\Omega\frac{dx(t)}{dt} \tag{2}$$

where m is the mass; c_x and c_y are the air damping coefficients; k_x and k_y are the spring constants of the driving beam and the sensing beam on x- and y-direction respectively; $x(t)$ and $y(t)$ are the displacement of the central mass on x- and y-direction respectively. Solving the above differential equations, we can have oscillatory motion in x- and y-direction.

$$x(t) = \frac{F_0}{c_x\omega_x}\sin \omega_x t \tag{3}$$

$$y(t) = \frac{2F_0\Omega}{c_x} \cdot \frac{1}{\sqrt{(\omega_y{}^2 - \omega_x{}^2)^2 + (c_y\omega_x / m)^2}} \cdot \sin(\omega_x t + \theta) \tag{4}$$

in which $\theta = \arctan\frac{\omega_y{}^2 - \omega_x{}^2}{c_y\omega_x / m}$, where ω_x and ω_y are the resonant frequencies for the x- and

y-directions respectively. We assume x_m and y_m are the amplitudes at resonance for the x- and y-directions. And we define $Q_x = \frac{m\omega_x}{c_x}$ and $Q_y = \frac{m\omega_y}{c_y}$ are the quality factors for x- and y-directions.

$$x_m = \frac{F_0 Q_x}{k_x} \tag{5}$$

$$y_m = \frac{2x_m\Omega}{\omega_y} \cdot \frac{\omega_x/\omega_y}{\sqrt{\left[1-\left(\omega_x/\omega_y\right)^2\right]^2 + \frac{1}{Q_y^2}\left(\omega_x/\omega_y\right)^2}} \tag{6}$$

$$\theta = \arctan \frac{1-\left(\omega_x/\omega_y\right)^2}{\frac{1}{Q_y}\cdot\left(\omega_x/\omega_y\right)} \tag{7}$$

When resonant frequency in x-direction and y-direction is precisely matched, which means $\theta = 0$, the mass oscillates along a linear path at an angle to the x-axis, as shown in Figure 2.

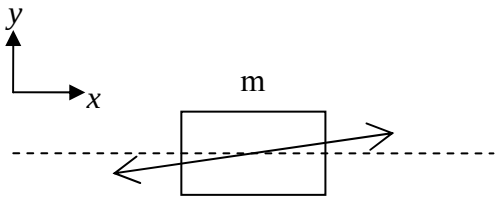

Figure 2. Oscillatory motion of mass for $\theta = 0$

The displacement sensitivity is

$$S_d = \frac{dy_m}{d\Omega} = \frac{2x_m}{\omega_y} \cdot \frac{\omega_x/\omega_y}{\sqrt{\left[1-\left(\omega_x/\omega_y\right)^2\right]^2 + \frac{1}{Q_y^2}\left(\omega_x/\omega_y\right)^2}} \tag{8}$$

The normalized displacement sensitivity is

$$S_{dn} = \frac{\omega_y}{2x_m} \cdot S_d = \frac{\omega_x/\omega_y}{\sqrt{\left[1-\left(\omega_x/\omega_y\right)^2\right]^2 + \frac{1}{Q_y^2}\left(\omega_x/\omega_y\right)^2}} \tag{9}$$

Figure 3 shows the relationship between the normalized sensitivity S_{dn} and (ω_x/ω_y) for different Q_y values.

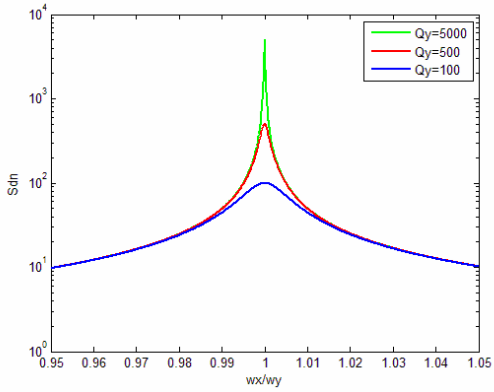

Figure 3. S_{dn} *versus* (ω_x/ω_y) *for different* Q_y *values*

From the curves we can see that the displacement sensitivity takes its peak value at $(\omega_x / \omega_y) = 1$, which indicates that in order to ensure the high sensitivity, we need to precisely match the resonant frequencies of driving and sensing mode. With the increase of Q_y, the peak becomes narrower and sharper, which indicate that increasing quality factors is another way to improve sensitivity.

III. Device design

The bulk-micromachined comb vibratory gyroscope design is shown in Figure 4. The microgyroscope is based on glass-silicon-glass compound structure through silicon-glass anodic bonding technique. The DRIE technique is use for comb finger etching, so that the device thickness can reach 100 um. The dark areas are anchored to the glass substrate, and the areas in light color are floating 10 um above the substrate and free for vibration. The microgyroscope consists of both driving and sensing portions. The left driving fingers, the right driving fingers and the truss are connected to the anchors through folded driving beams. The folded driving beam structure can help increase the amplitude of the driving vibration. The sensing portion consists of four sensing beams and a central mass. Similarly, the folded sensing beam structure can help increase the amplitude of the sensing vibration. The central movable mass constitutes differential sensing capacitances with top and bottom aluminum electrode deposited on the glass substrates. The upper and lower bonding anchors offer protection for the movable part.

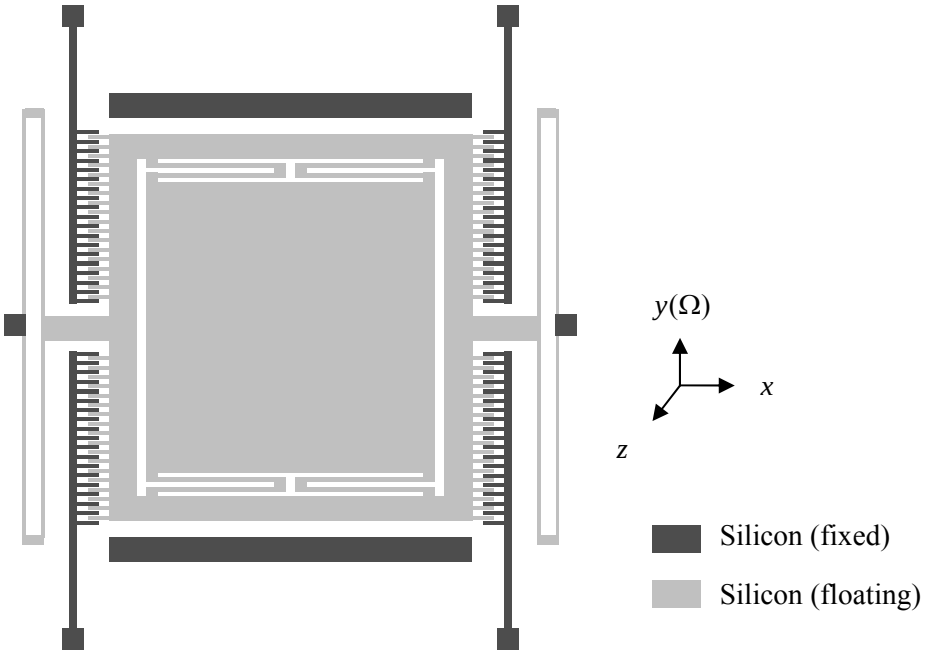

Figure 4. Middle silicon structure of the vibratory comb microgyroope

During operation, AC driving voltage V_1 and V_2 are applied to the left and right fixed driving fingers. This induces alternating electrostatic forces on the movable driving fingers along X direction in a "push-pull" mode. The truss along with central mass will vibrate along X direction, which we call driving mode. The frequency of the driving voltages is chosen to activate the truss and central mass in its resonant mode in order to achieve large vibration amplitude. If there is an angular velocity along Y direction, the central mass will experience an alternating Coriolis force along Z direction. This in turn will activate the central movable mass to vibrate along Z direction, which we call sensing mode. The sensing differential pair will change due to the sensing vibration along Z direction. By measuring this differential capacitance change, we know the value of the angular velocity.

IV. Performance

From Equation (4) we can see that the displacement sensitivity in detection mode is determined by resonant frequencies ω_x, ω_y, and air damping coefficients c_x, c_y. Therefore, to investigate the performance of the microgyroscope, we need to analyze these parameters.

Resonant frequency of a vibrating system is closely related to the spring constant of the spring-mass model. In our design, the truss with central mass connected to the driving beams of the gyroscope can be treated as a simplified spring-mass model. Four folded-beams can be treated as four springs connected in parallel. For each folded-beam, both sections of the beams can be treated as two springs connected in series. Each beam section can be applied as double-clamped beam model. The case for the central mass connected sensing beams are similar.

Spring constant k_{b_d} of one section of the driving beams can be calculated using double-clamped beam spring constant equation

$$k_{b\_d} = \frac{12EI_{b\_d}}{L_{b\_d}^{3}}$$

where I_{b_d} is the inertial momentum of the driving beam

$$I_{b\_d} = \frac{1}{12} t_{b\_d} W_{b\_d}^{3}$$

Two sections in a folded driving beam are connected in series and have the same size. Thus, spring constant of one folded driving beam is

$$k_{fold\_d} = \frac{1}{2} k_{b\_d} = \frac{6EI_{b\_d}}{L_{b\_d}^{3}}$$

Four folded driving beams are connected in parallel and have the same size. Thus, total spring constant in driving direction is

$$k_x = 4k_{fold\_d} = \frac{24EI_{b\_d}}{L_{b\_d}^{3}} = \frac{2Et_{b\_d} W_{b\_d}^{3}}{L_{b\_d}^{3}} \tag{10}$$

Total spring constant in detection direction can be expressed in a similar way, only the $t_{b\_d} W_{b\_d}^{3}$ in nominator is changed to $W_{b\_s} t_{b\_s}^{3}$ because the beams are deflected in the direction of thickness.

$$k_y = \frac{2EW_{b\_s} t_{b\_s}^{3}}{L_{b\_s}^{3}} \tag{11}$$

According to the definition of resonant frequency,

$$f_x = \frac{1}{2\pi}\sqrt{\frac{k_x}{M_d}} = \frac{1}{2\pi}\sqrt{\frac{2Et_{b\_d} W_{b\_d}^{3}}{M_d L_{b\_d}^{3}}} \tag{12}$$

$$f_y = \frac{1}{2\pi}\sqrt{\frac{k_y}{M_s}} = \frac{1}{2\pi}\sqrt{\frac{2EW_{b\_s} t_{b\_s}^{3}}{M_s L_{b\_s}^{3}}} \tag{13}$$

where M_d is the driving mass, including the mass of movable driving comb fingers, truss, sensing beams and central sensing mass; M_s is the mass of central sensing mass.

From Equation (12)-(13), we can see that: (1) resonant frequency decrease as the beam length increase; (2) resonant frequency increase as the beam width increase; (3) resonant frequency increase as the beam thickness increase; (4) driving mode frequency is more sensitive to beam length and width, less sensitive to beam thickness; (4) sensing mode frequency is more sensitive to beam length and thickness, less sensitive to beam width. Figure 5 shows the relationship between resonant frequency in x-/y-direction and their beam sizes, respectively.

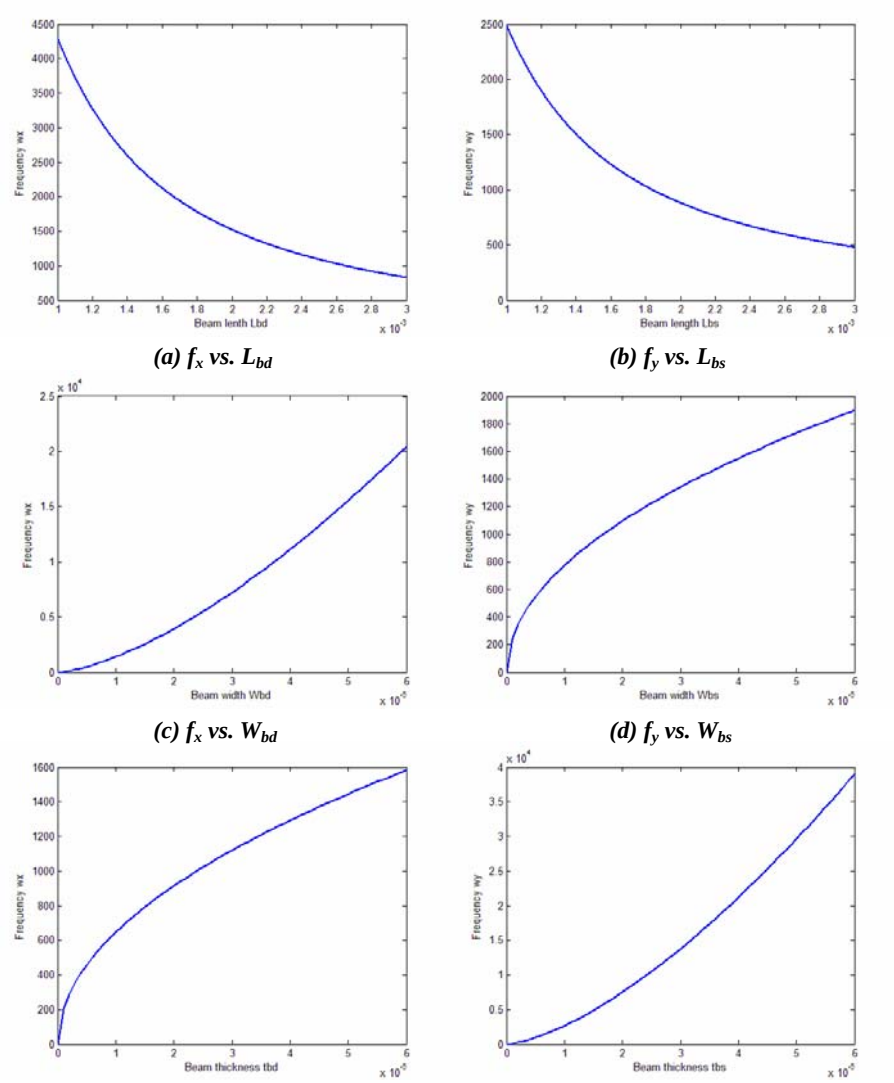

(a) f_x vs. L_{bd} ***(b) f_y vs. L_{bs}***

(c) f_x vs. W_{bd} ***(d) f_y vs. W_{bs}***

(e) f_x vs. t_{bd} ***(f) f_y vs. t_{bs}***

Figure 5. Beam length, width, thickness vs. resonant frequency

By properly adjusting the beam length, width and thickness of the gyroscope, we can modulate the resonant frequency of the device. Theoretically, higher frequency indicates a more stable system. We can narrow down the beam length or extend the beam width and thickness to achieve very high device resonant frequency. However, the device sensitivity may also be affected when the beam size is changed. Figure 6 shows the relationship between displacement sensitivity and their beam sizes. We can see that: (1) displacement sensitivity increase as the beam length increase; (2) displacement sensitivity decrease as the beam width increase; (3) displacement sensitivity decrease as the beam thickness increase. Therefore, there is a trade-off between device resonant frequency and sensitivity, and we may choose a moderate beam size to make both of them meet the minimum requirement.

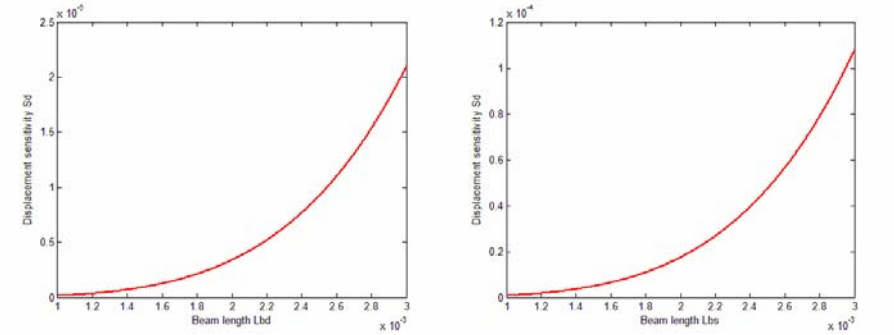

(a) S_d vs. L_{bd} ***(b) S_d vs. L_{bs}***

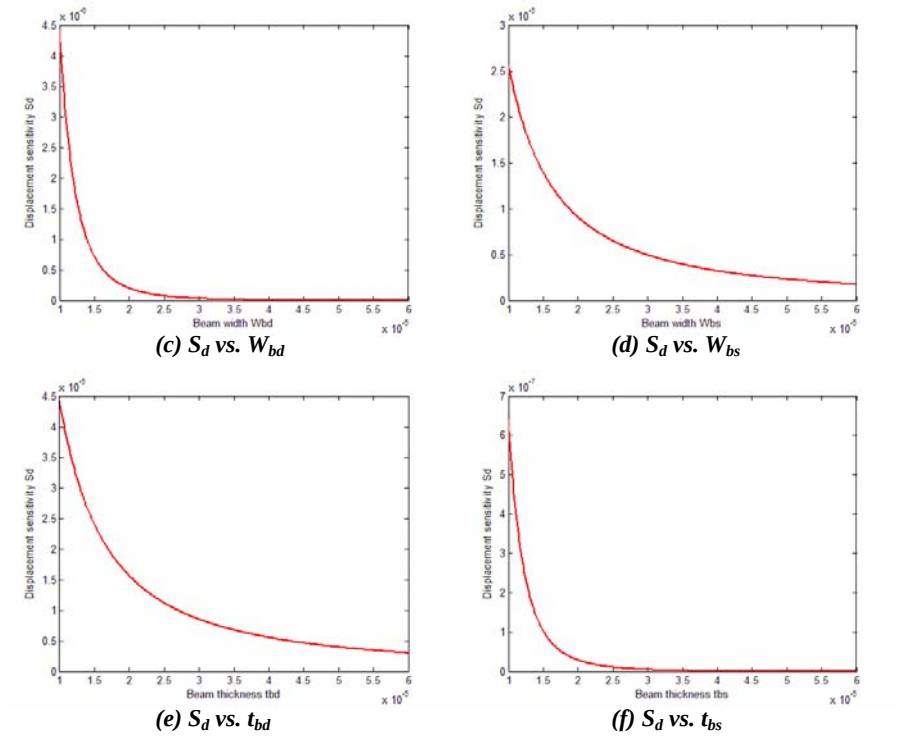

(c) S_d vs. W_{bd} *(d) S_d vs. W_{bs}*

(e) S_d vs. t_{bd} *(f) S_d vs. t_{bs}*

Figure 6. Beam length, width, thickness vs. displacement sensitivity

The microgyroscope uses a differential capacitance pair to detect the displacement of central mass in Z direction, as shown if figure 7.

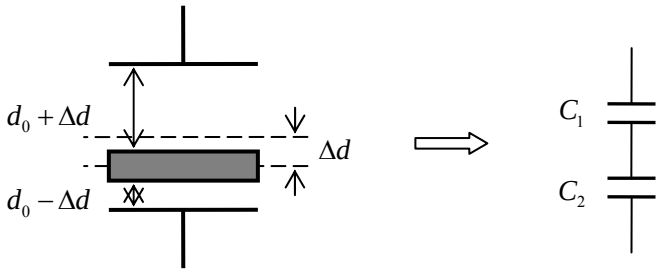

Figure 7. Differential capacitance pair in MEMS gyroscope

When there is no AC driving voltage or angular velocity, the static sensing capacitance of the MEMS gyroscope is

$$C_0 = \frac{\varepsilon S}{d_0} \tag{16}$$

where ε is the dielectric constant of air; S is the area of aluminum electrode; d_0 is the static capacitance gap between central mass and electrode. Assume there is a Coriolis force making the central mass move downward by Δd, as shown in Figure 7. Assume small deflection approximation $\Delta d \ll d_0$, the top (bottom) capacitances C_1 (C_2) are changed to

$$C_1 = \frac{\varepsilon S}{d_0 + \Delta d} = \frac{\varepsilon S}{d_0\left(1 + \Delta d / d_0\right)} \approx \frac{\varepsilon S}{d_0}\left(1 - \frac{\Delta d}{d_0}\right)$$

$$C_2 = \frac{\varepsilon S}{d_0 - \Delta d} = \frac{\varepsilon S}{d_0\left(1 - \Delta d / d_0\right)} \approx \frac{\varepsilon S}{d_0}\left(1 + \frac{\Delta d}{d_0}\right)$$

The differential capacitance change ΔC is

$$\Delta C = C_2 - C_1 = \frac{2\varepsilon S}{d_0} \cdot \left(\frac{\Delta d}{d_0} \right) = 2C_0 \left(\frac{\Delta d}{d_0} \right) \tag{17}$$

From above equations we can see that for small deflection approximation (beam deflection angle smaller than 5°), differential capacitance change is directly proportional to the displacement of the movable mass.

V. Optimization

Based upon the above analysis, an optimized design of MEMS gyroscope is achieved. Some design parameters are shown in Table 1. Assume $Q_x = 200$ and $Q_y = 200$, the device performance parameters are shown in Table 2.

Table 1. The optimized design parameters of the microgyroscope

Design Parameters	**Values**
Device dimension	5.8mm×6.0mm
Device thickness	100μm
Driving beam length L_{bd}	1770μm
Driving beam width W_{bd}	12μm
Driving beam thickness t_{bd}	80μm
Sensing beam length L_{bs}	1200μm
Sensing beam width W_{bs}	60μm
Sensing beam thickness t_{bs}	8μm
Central mass length L_m	3000μm
Central mass width W_m	3000μm
Central mass thickness t_m	80μm
Comb finger length L_f	200μm
Comb finger width W_f	40μm
Comb finger thickness t_f	80μm
Total number of driving fingers N_f	80
Driving capacitance gap d_f	3μm
Sensing capacitance gap d_0	10μm
Truss width	250μm
Truss thickness	80μm
Anchor size	200μm×200μm
Aluminum electrode size	2.8mm×2.8mm
Bonding anchor length	3.7mm
Bonding anchor width	0.3mm

Table 2. The performance parameters of the microgyroscope

Performance Parameters	**Values**
Static capacitance C_0	6.942pF
Driving mass M_d	1.678mg
Sensing mass M_s	2.570mg
Driving mode spring constant k_x	8.476N/m
Sensing mode spring constant k_y	6.044N/m
Driving mode resonant frequency f_x	289.017Hz
Sensing mode resonant frequency f_y	302.102Hz
Displacement sensitivity S_d	105.9nm/(°/sec)
Capacitance sensitivity S_c	6.942fF/(°/sec)

From Table 2, we can see that resonant frequency of the driving and sensing modes are $f_x = 289.0Hz$ and $f_y = 302.1Hz$ separately. Due to process variation, the fabrication may cause deviations in resonant frequencies of driving and sensing modes, even if we precisely match them in theoretical calculation. Hence here we intentionally set f_y to be 3.8% larger than f_x. Then a DC biasing voltage can be used to tune down f_y in differential capacitance sensing to precisely match the value of f_x. During operation, the DC biasing voltage will introduce a negative spring constant to the spring mass model

$$\Delta k = -\frac{2\varepsilon S V_d^{\,2}}{d_0^{\,3}}$$

If electrostatic tuning is applied to k_y, the effective resonant frequency in sensing mode after applying the DC biasing voltage can be expressed as

$$f_e = \frac{1}{2\pi}\sqrt{\frac{k_y - \Delta k}{M_s}} = f_y\left(1 - \frac{\varepsilon S V_d^{\,2}}{k_y d_0^{\,3}}\right) \tag{18}$$

From the analysis above, we can derive the expected effective resonant frequency f_e of the microgyroscope under a certain biasing DV voltage V_d, as shown in Figure 8. When there is no biasing voltage, $f_e = f_y = 302.1\text{Hz}$; when there is a 5V biasing voltage, we can tune down the f_e to 215.4Hz, which is significantly decreased compared to the original value; when there is a 1.94V biasing voltage, we may achieve $f_e = f_x = 289.0\,\text{Hz}$, thus eliminating the frequency mismatch.

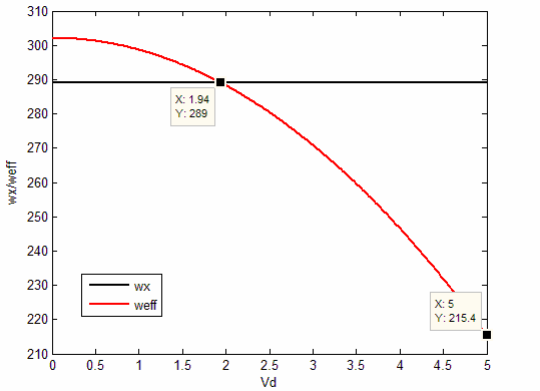

Figure 8. Effective resonant frequency under a certain DC biasing voltage

VI. Simulation

The above theoretical analysis predicts the relationship between device resonant frequency and various design parameters (such as beam length, beam width and beam thickness). However, the theoretical analysis is based on the simplified spring-mass model. In order for a more accurate analysis, ANSYS FEM simulation [13] is required to simulate the device resonant frequencies in driving and sensing modes. The deform-shaped ANSYS models for an optimized design of the MEMS comb gyroscope are shown in Figure 9 and Figure 10. Here only the movable parts and the anchors are shown in the figures. The fixed comb fingers do not contribute to the resonant frequency of the movable parts, thus they are not shown in the figures.

Based on ANSYS simulation, the resonant frequencies in driving and sensing modes are extracted: fx=617.37Hz and fy=675.46Hz. These results can be very helpful for guiding future research and microfabrication. The simulated results have a considerable difference with the theoretical calculation fx=289.0Hz and fy=302.1Hz. This is because the beam and mass structure is simplified as an ideal spring-mass model, in which the geometric dimension of the mass and mass of the beams are neglectable. However, in our device, the vibration system has a distributed mass. Also ANSYS FEM

simulation takes residual stress, real anchor and plate compliance into consideration, therefore gives a result more close to experimental data [14].

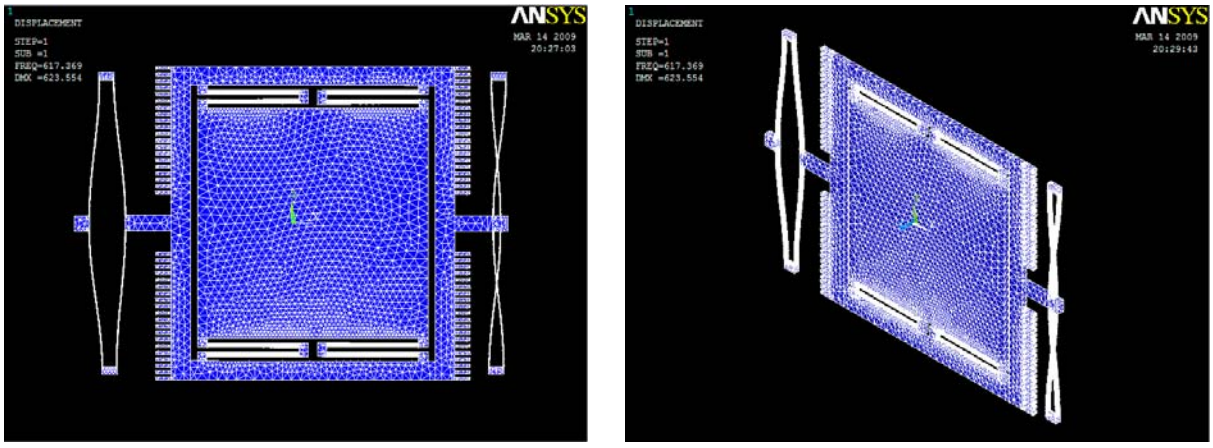

(a) Top view ***(b) Isometric view***

Figure 9. ANSYS model of MEMS gyroscope in driving mode (shape exaggerated)

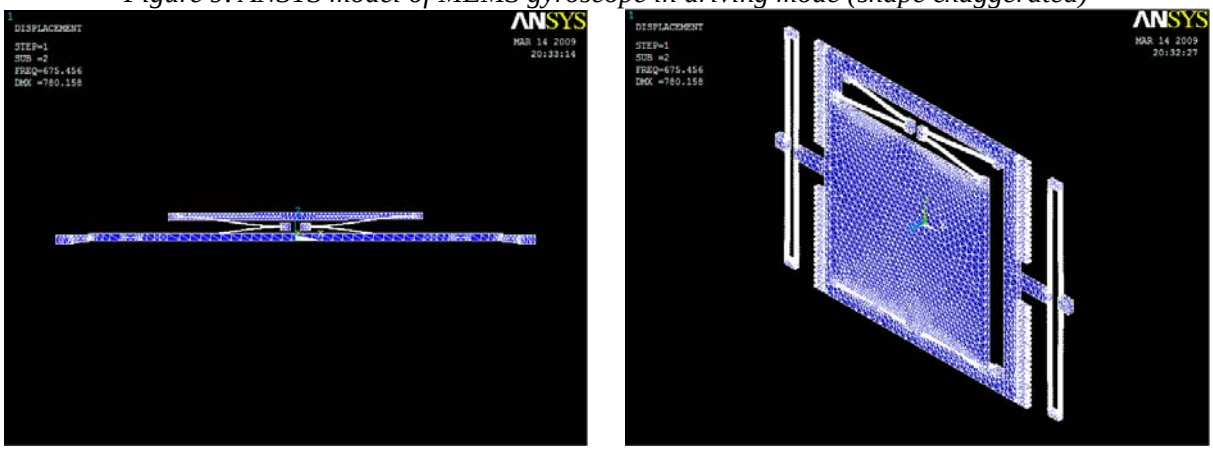

(a) Front view ***(b) Isometric view***

Figure 10. ANSYS model of MEMS gyroscope in sensing mode (shape exaggerated)

VII. Fabrication Process

This MEMS gyroscope fabrication is simple. The fabrication process is shown in Figure 11. The deep reactive-ion etching technique increases the device thickness to 100um, which greatly increase the device capacitance and improve the device operation stability. Glass substrates are bonded to silicon structure using silicon-glass anodic bonding technique. The glass substrates help to minimize the parasitic capacitance, and limit the maximum range of the displacement of sensing mass in case of z-axis over loading, which is helpful in shocking environment.

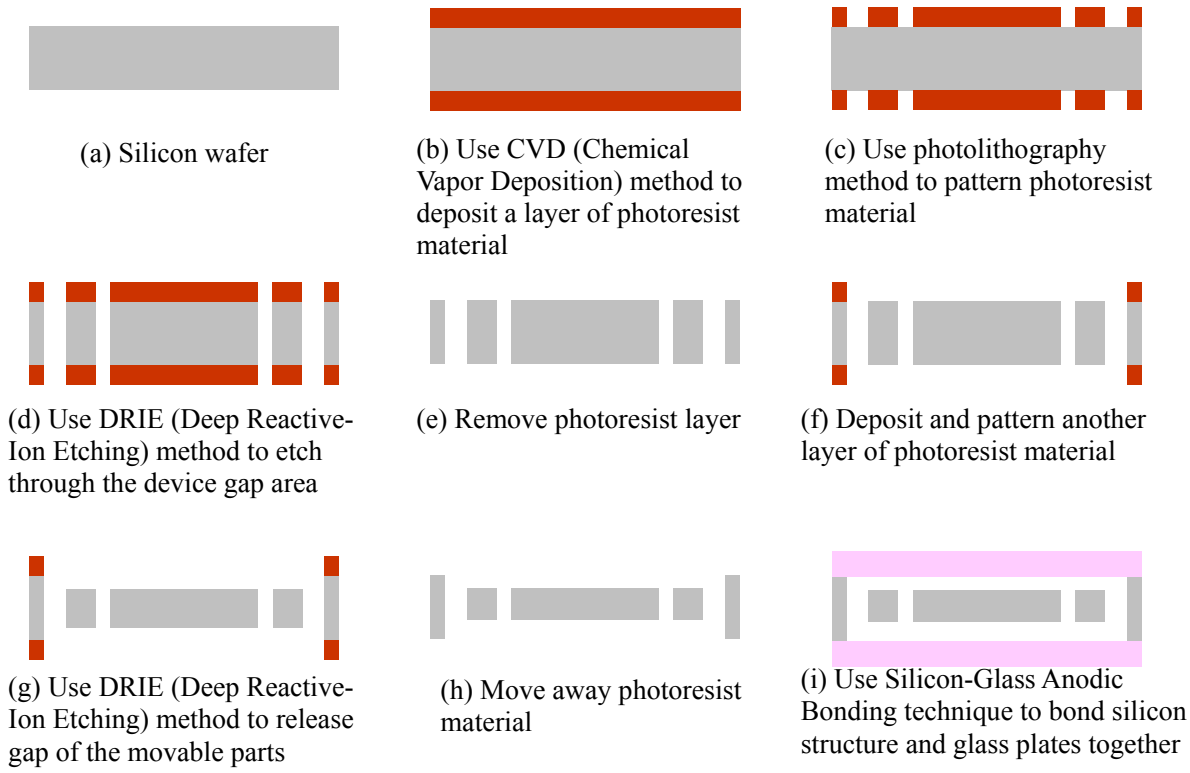

Figure 11. Fabrication process of the microgyscope

VIII. Conclusion

In this paper, a novel bulk-micromachined comb vibratory microgyroscope design is proposed. The gyroscope uses electrostatic comb driving for its driving mode, and differential plate capacitance sensing for signal detection. The device is based on silicon-on-glass structure. DRIE technique is used to increase the device thickness to 100um. The working principle and performance of the microgyroscope are analyzed in detail. Based upon the analysis, an optimized microgyroscope design is proposed. Simulation results demonstrate the gyroscope has the resonant frequency of 617.37Hz and 675.46Hz in driving and sensing mode. Theoretical calculation shows that the device has the displacement sensitivity of 105.9nm/(°/sec) and capacitance sensitivity of 6.942fF/(°/sec). The microgyroscope is attractive for its good performance and ease for fabrication.

The future work is to simulate the displacement sensitivity and capacitance sensitivity of this microgyroscope in ANSYS software, and see how it is matched with the theoretical calculation. Also, we will try to further improve the performance of this proposed microgyroscope by using novel design structure (e.g. four-fold beam). We will look into how to achieve optimized design with these design improvements.

References

[1]. URL: http://en.wikipedia.org/wiki/MEMS_gyroscope
[2]. N. Maluf and K. Williams, "An Introduction to Microelectromechanical Systems Engineering", *Artech House, Inc.*, Norwood, MA, USA, 2004.
[3]. S. Nasiri, "A Critical Review of MEMS Gyroscopes Technology and Commercialization Status", *Inven. Sense*, CA, 2005.
[4]. K. Tanaka, Y. Mochida, M. Sugimoto, K. Moriya, T. Hasegawa, K. Atsuchi and K. Ohwada, "A Micromachined Vibrating Gyroscope", *Sensors & Actuators A: physical*, Vol. 50, pp.111-115, 1995.

[5]. Y. Oh, B. Lee, S. Baek, H. Kim, J. Kim, S. Kang, C. Song, "A Tunable Vibratory Microgyroscope ", *Sensors & Actuators A: physical*, Vol. 64, pp.51-56, 1998.
[6]. X. Xiong, D. Lu and W. Wang, "A Bulk-micromachined Comb Vibrating Microgyroscope Design", *the 48th IEEE International Midwest Symposium on Circuits & Systems*, Vol.1, pp. 151-154, Cincinnati, Ohio, USA, Aug 7-10, 2005.
[7]. Y. Liang, T. Zhao, Y. Xu and S. Boh, "A CMOS Fully-integrated Low-voltage Vibratory Microgyroscope", *IEEE Region 10 International Conference on Electrical and Electronic Technology*, Vol. 2, pp.825-828, 2001.
[8]. B. Yeh and Y. Liang, "Modeling and Compensation of Quadrature Error for Silicon MEMS Microgyroscope", *the 4th IEEE International Conference on Power Electronics and Drive Systems*, Vol. 2, pp.871-876, 2001.
[9]. Y. Mochida, M. Tamura and K. Ohwada, "A Micromachined Vibrating Rate Gyroscope with independent beams for the drive and detection modes", *Sensors & Actuators A: physical*, Vol. 80, pp.170-178, 2000.
[10]. S. Bhave, J. Seeger, X, Jiang, B. Boser, B. Roger, T. Howe and J. Yasaitis, "An Integrated, Vertical-drive, In-plane-sense Microgyroscope", *the 12th International Conference on Transducers, Solid-state Sensors, Actuators and Microsystems*, Vol. 1, pp.171-174, 2003.
[11]. H. Song, Y. Oh, I. Song, S. Kang, S. Choi, H. Kim, B. Ha, S. Baek and C. Song, "Wafer Level Vacuum Packaged De-coupled Vertical Gyroscope by a New Fabrication Process", *the 15th Annual International Conference on Micro Electro Mechanical Systems*, pp.520-524, 2000.
[12]. M. Bao, "Analysis and Design Principles of MEMS Devices", *Elsevier Inc.*, San Diego, CA, USA, 2005.
[13]. URL: http://www.ansys.com
[14]. M. Lishchynska, N. Cordero, O. Slattery and C. O'Mahony, "Spring Constant Models for Analysis and Design of MEMS Plates on Straight or Meander Tethers", *Sensor Letters*, Vol. 4, pp.200-2005, 2006.
[15]. K. Sharma, I. Macwan, L. Zhang, L. Hmurcik, X. Xiong, "Design Optimization of MEMS Comb Accelerometer", *American Society for Engineering Education Zone 1 Conference*, 2008.

Biographies

Haifeng Dong is a master student in Department of Electrical and Computer Engineering, University of Bridgeport, USA. He received his B.S. degree in Electronics and Information Engineering from the Tongji University, Shanghai, China in 2005. His current research area includes MEMS (Micro-Electro-Mechanical Systems), analog VLSI and low power VLSI circuits.

Dr. Xingguo Xiong is an assistant professor in Department of Electrical and Computer Engineering, University of Bridgeport, CT. He received his Ph.D degree in electrical engineering from Shanghai Institute of Microsystem and Information Technology, China, in 1999. He received his second Ph.D degree in computer engineering from University of Cincinnati, OH, USA in 2005. His research interests include microelectromechanical system (MEMS), nanotechnology, as well as VLSI design and testing.